Gong, Hanyang; Polojärvi, Arttu; Tuhkuri, Jukka

Discrete Element Simulation of the Resistance of a Ship in Unconsolidated Ridges

Published in:
Cold Regions Science and Technology

DOI:
10.1016/j.coldregions.2019.102855

Published: 01/11/2019

Document Version
Publisher's PDF, also known as Version of record

Please cite the original version:
Gong, H., Polojärvi, A., & Tuhkuri, J. (2019). Discrete Element Simulation of the Resistance of a Ship in Unconsolidated Ridges. *Cold Regions Science and Technology*, *167*, Article 102855.
https://doi.org/10.1016/j.coldregions.2019.102855

Journal Pre-proofs

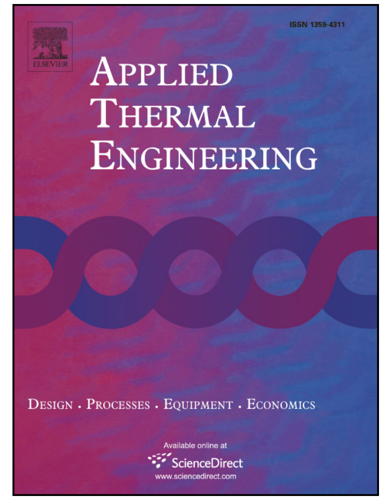

Heat Transfer Modeling of a Parabolic Trough Solar Collector with Working Fluid of Fe_3O_4 and CuO/Therminol 66 Nanofluids under Magnetic Field

Mohammad Malekan, Ali Khosravi, Sanna Syri

PII: S1359-4311(19)31979-9
DOI: https://doi.org/10.1016/j.applthermaleng.2019.114435
Reference: ATE 114435

To appear in: *Applied Thermal Engineering*

Received Date: 25 March 2019
Revised Date: 12 August 2019
Accepted Date: 23 September 2019

Please cite this article as: M. Malekan, A. Khosravi, S. Syri, Heat Transfer Modeling of a Parabolic Trough Solar Collector with Working Fluid of Fe_3O_4 and CuO/Therminol 66 Nanofluids under Magnetic Field, *Applied Thermal Engineering* (2019), doi: https://doi.org/10.1016/j.applthermaleng.2019.114435

Heat Transfer Modeling of a Parabolic Trough Solar Collector with Working Fluid of Fe_3O_4 and CuO/Therminol 66 Nanofluids under Magnetic Field

Mohammad Malekan [1], Ali Khosravi [2,*], Sanna Syri[2]

[1] Department of Engineering, Aarhus University, Denmark
[2] Department of Mechanical Engineering, School of Engineering, Aalto University, Finland
* Corresponding author: ali.khosravi@aalto.fi

Abstract

Solar energy is among the cleanest and most adaptable compared to other renewable energy sources. The major challenge is how to get this energy in efficient way to make it available for industrial applications such as electricity generation. One of the most efficient techniques to harvest solar energy and transform it into electrical energy is parabolic trough solar collector (PTSC), which is a type of concentrating solar power generation systems. This system operates by concentrating solar irradiance onto a tubular receiver in which this centralized energy is absorbed by a heat transfer fluid and transported to the power cycle. Improving the performance of the PTSC can enhance efficiency as well as power generation of a PTS power plant. Hence, this issue has been considered as one of the major challenges for scholars in this field. One promising solution is finding more efficient heat transfer working fluids. Another suggestion is proposing a different geometry for the receiver. In the current research, ferrofluids due to their heat transfer characteristics are proposed as working fluid for a PTSC. Fe_3O_4/Therminol 66 and CuO/Therminol 66 nanofluids are examined under external magnetic field for this target. Besides, to improve the heat transfer characteristics of the collector, the receiver is designed with internal fins. This work is carried out using computational fluid dynamics (CFD). The assessments are done by considering the different nanoparticle sizes on the friction factor, thermal efficiency, performance evaluation criteria (PEC) and convective heat transfer.

The results depict that reducing the particle size and enhancing the nanoparticles volume fraction increase the convective heat transfer coefficient, Nusselt number, PEC and the collector efficiency. In addition, the collector efficiency rises in the attendance of the magnetic field and maximum efficiency of the collector was obtained for 4% Fe_3O_4/Therminol 66 working fluid.

Keywords: CFD simulation; Parabolic trough collector; Fe_3O_4 and CuO nanoparticles; Heat transfer coefficient; Magnetic field; Smooth and finned tubes

1. Introduction

The use of fossil fuels due to their adverse effects on the environment, global warming and climate change needs to be reduced [1]. Hence researchers strive to attain independence from such sources of energy and move towards alternative and renewable sources like geothermal, wind and specifically solar energy (SE) [2], [3]. Among them, SE is the most abundant and easily accessible. Although many engineering systems have been designed to catch and absorb the SE (such as photovoltaic system and solar thermal facilities), it is crucial to make these alternative technologies more efficient [4]. Research into solar thermal systems has provided us with high-efficiency solar collectors, which research is continuing aiming to further enhance efficiency.

Although solar photovoltaic system is recognized as one of the most commercialized technologies for harnessing SE, solar thermal has some striking advantages such as: designing a thermal energy storage system (using molten salt) to produce the electricity during night, benefiting of a wide range of solar radiation, and durability against damage during intense radiation and operation under high temperature [5]–[7]. A parabolic trough solar collector

(PTSC) is a type of solar thermal power generation systems in which the SE is harvested using a parabolic mirror and concentrated onto a long metal tube [8], [9]. In this system, the concentrated solar radiation onto the tube is received by the working fluid and then it is utilized to generate steam for the Rankine cycle. A parabolic trough collector commonly uses thermic oils like Syltherm, Dowtherm, Therminol, and Sandotherm where Therminol VP1 and Syltherm 800 due to their reliability and accessibility are more applicable [10].

Nomenclature

A_a	collector aperture	μ_0	magnetic permeability constant in vacuum
B	magnetic field	μ_t	turbulent viscosity
bf	base fluid	Nu	Nusselt number
$C_{1\varepsilon}$, $C_{2\varepsilon}$	constants	Nu_0,	receiver Nusselt number based on base fluid
C_R	collector concentration ratio	p	particle
D	characteristic length	PEC	performance evaluation criteria
ΔP	pressure drop	Q_s	solar irradiance over the collector
ε	dissipation rate	Q_u	useful heat
η_{th}	thermal efficiency	r	Interval between wire position and tube
f	friction factor	Re	Reynolds number
f_0	receiver friction factor based on base fluid	σ_k, σ_ε	turbulent Prandtl numbers for k and ε
ff	ferrofluid	T_{in}, T_{out}	inlet and outlet temperatures
φ	volume fraction	u	fluid velocity
G_b	direct beam solar irradiation		
G_k	turbulence kinetic energy generation	*Abbreviations*	
h	convective heat transfer coefficient	CFD	Computational fluid dynamics
H_x, H_y	magnetic fields in x and y directions	CHT	Convective heat transfer
I	electric current	DPHX	Double pipe heat exchanger
I_b	beam radiation	HTC	Heat transfer coefficient
I_g	global radiation	LCOE	Levelized cost of energy
K	thermal conductivity coefficient	MF	Magnetic field
k	turbulent kinetic energy	MWCNT	Multi-wall carbon nanotube
L	length of tube	PTSC	Parabolic trough solar collector
$\dot{m}$	mass flow rate	PTC	Parabolic trough collector
μ	dynamic viscosity	RNG	Re-normalisation group

Nanofluids are a unique class of industrial fluids that are composed by addition of nanoparticles (for instance Al_2O_3, CuO, Fe_3O_4, and SiO_2) into the common industrial fluids like water and oil [11]. Nanofluids possess exhibited high thermal conductivity and promising thermal characteristics compared to conventional industrial fluids. For PTSCs, many investigations have proposed and evaluated different nanofluids as working fluid. Tagle-Salzar et al. [12] developed an experimental study to assesses the thermal proficiency of the PTSC with Al_2O_3-water nanofluid. It was obtained that the quantity thermal enhanced when Al_2O_3 nanoparticles were added into base fluid. For one collector this increasing has been reported as 0.3% for heat gain and 0.03% for thermal efficiency. Khakrah et al. [13] implemented an exergy analysis for a PTSC with working fluid of Al_2O_3/synthetic oil. It was found out that utilizing nanoparticles with 5% volume fraction enhances the relative exergy efficiency approximately around 19%. Korres et al. [14] evaluated the thermal efficiency of a PTSC with Syltherm 800/CuO (nanoparticle concentration:5%) working fluid. They have shown that the medium and uttermost heat transfer coefficient (HTC) improvements were 16.16% and 17.41%, respectively. In addition, they have shown that the values of pressure drop as well as the pumping work demand for nanofluid in all cases were too low. Shafiey and Zamani [15] examined MgO nanofluids to improve the thermal efficiency of a heat pipe solar collector. They reported that enhancing the mass flow rate inside the collector increased its thermal efficiency. Moreover, the HTC of solar collector enhanced when nanofluids were applied instead of the base fluids. Sharafeldin and Grof [16] proposed WO_3/water nanofluid for an evacuated tube solar system and obtained that the heat gain and solar collector outlet temperature increased with 23% and 21%, respectively. Tafarroj et al. [17] analyzed the proficiency of a PTSC for nanofluids through CFD simulation and artificial neural network. Nanosilica and multi-wall carbon nanotube (MWCNT) were mixed together with ethylene glycol as the base fluid. Their results depicted that the nanofluid containing 0.6% MWCNT had the maximum temperature outlet.

Besides, in this area, molten salts with nanoparticles (nano-salts) have been evaluated extensively by many scholars. Yaxuan et al. [18] performed an analysis to enhance the performance of bromide salt by nano-particle dispersion employed for high-temperature heat pipes in concentrated solar systems. They reported that decomposing point and heat of fusion were enhanced by 68.4 ℃ and 99.19%, respectively. Wei et al. [19] ameliorated the thermal conductivity of liquid nitrate and carbonate salts doped with MgO particles. It was derived that the thermal diffusivity of nitrate salt and carbonate salt remarkably improved with the augmentation of MgO particles. In another study, specific heat of silica nanofluid was improved by Shin and Banerjee [20].

Ferrofluids are defined as liquids containing single-domain nanoparticles (for instance iron nickel oxide, cobalt and their oxides, ferric oxide, etc.) with an average diameter of 15 nm or less. Ferrofluids are simulated through ferrohydrodynamic governing equations under magnetic field (MF). As we know, thermal conductivity of metals is higher than liquids. Hence, it will be predicted ferrofluids that are a colloidal mixture of magnetic metal particles in a base fluid perform better than the conventional industrial fluids in thermal characteristics. Various numerical efforts have been made to assess the thermal performance of ferrofluids with/without the attendance of MF. Malekan and Khosravi [21] assessed the result of MF upon the HTC of Fe_3O_4/water nanofluid trough an intelligent model called adaptive neuro-fuzzy inference system optimized with particle swarm optimization, and CFD simulation. It was derived that the presence of MF can enhance the HTC of ferrofluid. Malekan et al. [22] enhanced the thermal efficiency of a double pipe heat exchanger (DPHE) incorporated with a small scale CAES (compressed air energy storage) system by considering a ferrofluid as secondary fluid for the exchanger. Khosravi et al. [10] proposed Fe_3O_4-Therminol 66 (the examined volume fraction (1-4%)) at presence of magnetic field (0-500 G) as working fluid for a PTSC. Their results have illustrated that using MF improves the thermal characteristics of the solar collector including thermal efficiency, HTC, and output temperature. In another research work, the HTC of nanofluids under MF was evaluated by Jafari et al. [23]. They assessed the heat transfer of nanofluids under MF in a helical DPHX and for laminar stream in which increasing the HTC at presence of MF was reported. Khosravi and Malekan [24] developed intelligent methods to predict the HTC of Fe_3O_4/water ferrofluid in attendance of various MFs and operational conditions. Aminfar et al. [25], [26] assessed the hydro-dynamic and hydro-thermal manner of ferrofluids by using the non-uniform transverse/axial MF.

Based on the literature review, many articles have proposed nanofluids (such as Al_2O_3/water, SiO_2/water, TiO_2/water, etc.) as working fluids for PTSCs. Extensive research works have been carried out on the effect of MF on heat transfer of ferrofluids in diverse industrial purposes. It could be plainly viewed that in most of them Fe_3O_4 nanoparticle has been appraised for ferrofluid suspension. In the case of PTSC, CuO has been recommended as nanoparticle suspended in the base fluid. There is no study to figure out the thermal and fluid behavior of CuO under MF and this study has been intrigued to fill this knowledge gap. Indeed, this study provides a comparison between the CuO/Therminol 66 and Fe_3O_4/Therminol 66 under various MF for a PTSC. These investigations are undertaken while the central receiver is designed with internal fins. As a matter of fact, in the current study, for the first time, the distribution of the thermal and fluid flow characteristics of the mentioned ferrofluids impressed by

MF for the finned tube and smooth tube are compared and investigated. Besides, the impress of the particle size of nanoparticles on the thermal demeanor of the collector is determined. Moreover, this research illuminates the contribution of geometry changes against working fluid changes.

2. Methodology

2.1. Parabolic Trough Solar System

Commonly a PTSC power plant that commonly uses U-curved mirrors in order to harvest solar radiation. This system is classified between the concentrating solar systems in which the direct normal solar irradiance is collected and transformed to the thermic energy. This concentrated energy is received by the working fluid and its evaporating lead to electricity generation. In this research, in order to attain to solution for increasing the thermal efficiency of the solar collectors, ferrofluids are proposed and evaluated using CFD simulation. Generally, a PTSC power plant is incorporated with a solar field (filled with lots of solar collectors), power cycle (for instance a Rankine cycle), and in some cases, thermal energy storage system accompanied by fossil fuel backup system. The solar field includes the parabolic, trough-shaped collectors that navigate normal solar irradiance onto tubular receivers. Each collector contains the mirrors and its structure in order to support the receivers, mirrors as well as sun tracker system; and each receiver contains a metal pipe with a solar absorbing surface.

2.2. Model Definition

The utilized model in this work includes a solar thermal collector and a receiver tube, as demonstrated in Fig. 1(a). A non-uniform MF is generated by embedding an electrical wire parallel to the receiver tube axial direction, hereunder the tube. Further, Fig. 1(b) presents the approximate model of the local concentration ratio (C_R) for the receiver tube. This figure demonstrates that only the tube lower half receives the reflected solar radiation by the collector.

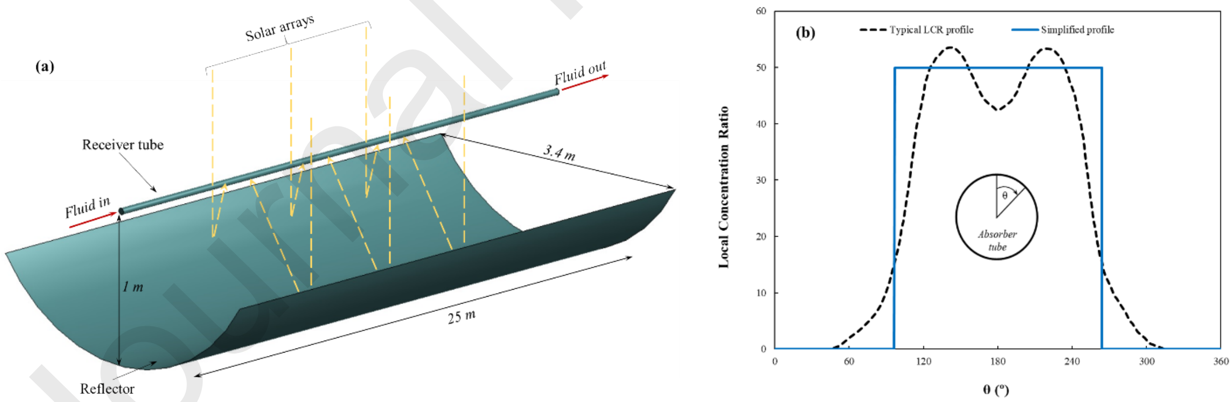

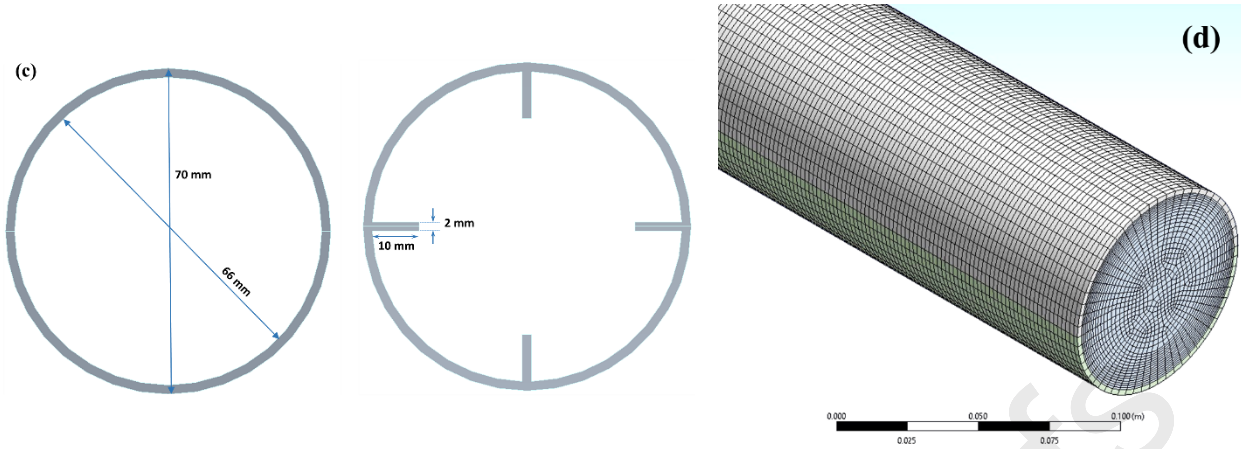

Fig. 1. (a) Schematic of the PTC model, (b) C_R distribution in the receiver, and (c) collector tube cross section, with and without fins, and (d) a typical grid discretization of the problem.

Area under curves of the simplified model and typical LCR profile from [27] show an error of less than 5%, which indicates the simplified model can be considered as a good approximation of the typical LCR profile. This simplified model was also proposed by Munoz et al. [28]. Two types of collector tubes are considered in this study, smooth and finned tubes as shown in Figure 1(c). These two configurations are considered to evaluate the effects of fins on the PTC performance with and without presence of MFs. In addition, a typical grid discretization of the receiver tube problem is shown in Figure 1(d).

2.1. Governing Equations under Presence of Magnetic Fields

Numerical analysis is done by coupling the equations of energy and Navier-Stokes to ascertain the heat transfer specifications inward the tube. The influence of MF is accounted by calculating the components of MF in the momentum equations. Continuity equation is defined as [29]:

$$\frac{\partial u}{\partial x}+\frac{\partial v}{\partial y}+\frac{\partial w}{\partial z}=0 \tag{1}$$

in which, following assumption were used to utilized continuity equation to numerically model the current nanofluid: steady, and incompressible and laminar nanofluid flow, thermo-physical properties to be constant, and viscosity loss to be negligible. Momentum equations are [29]:

$$\rho\left(u\frac{\partial u}{\partial x}+v\frac{\partial u}{\partial y}+w\frac{\partial u}{\partial z}\right)=-\frac{\partial p}{\partial x}+\mu\left(\frac{\partial^2 u}{\partial x^2}+\frac{\partial^2 u}{\partial y^2}+\frac{\partial^2 u}{\partial z^2}\right)+F_K(x) \tag{2}$$

$$\rho\left(u\frac{\partial v}{\partial x}+v\frac{\partial v}{\partial y}+w\frac{\partial v}{\partial z}\right)=-\frac{\partial p}{\partial y}+\mu\left(\frac{\partial^2 v}{\partial x^2}+\frac{\partial^2 v}{\partial y^2}+\frac{\partial^2 v}{\partial z^2}\right)+F_K(y) \tag{3}$$

$$\rho\left(u\frac{\partial w}{\partial x}+v\frac{\partial w}{\partial y}+w\frac{\partial w}{\partial z}\right)=-\frac{\partial p}{\partial x}+\mu\left(\frac{\partial^2 w}{\partial x^2}+\frac{\partial^2 w}{\partial y^2}+\frac{\partial^2 w}{\partial z^2}\right) \tag{4}$$

Energy equation is defined as [29]:

$$(\rho\, C_p)\left(u\frac{\partial T}{\partial x}+v\frac{\partial T}{\partial y}+w\frac{\partial T}{\partial z}\right)=k\left(\frac{\partial^2 T}{\partial x^2}+\frac{\partial^2 T}{\partial y^2}+\frac{\partial^2 T}{\partial z^2}\right) \tag{5}$$

where, $F_K(x)$ and $F_K(y)$ are Kelvin force (owing to the magnetic gradient). The components of Kelvin force are defined as $\mu_0 M\frac{\partial H}{\partial x}$ and $\mu_0 M\frac{\partial H}{\partial y}$ in x and y directions, respectively. These components are obtained as a result of the electric current through the wire. The position of this current-carrying wire and schematic of distribution of MFs are presented in Figure 2. The MF of electric current are H_x and H_y, in the x and y directions respectively, and are defined by the following equations [30]:

$$H_x(x,y) = \frac{I}{2\pi}\frac{(x-a)}{(x-a)^2+(y-b)^2} \tag{6}$$

$$H_y(x,y) = \frac{I}{2\pi}\frac{(y-b)}{(x-a)^2+(y-b)^2} \tag{7}$$

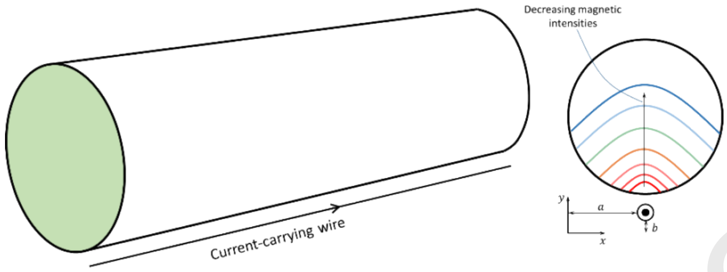

Fig. 2. Schematic of position of an electric wire accompany with the tube cross section which shows distribution of the MF.

The MF strength is calculated by [24], [29]:

$$H(x,y,z) = \frac{I}{2\pi}\frac{1}{\sqrt{(x-a)^2+(y-b)^2}} \tag{8}$$

Also, M is defined as magnetization and is obtained by [24], [29]:

$$M = \frac{6m_p}{\pi d_p^3}\left[coth(\xi) - \frac{1}{\xi}\right] \tag{9}$$

Where ξ is the Langevin parameter and can be obtained by the following formula [24], [29]:

$$\xi = \frac{\mu_o m_p H}{K_B T} \tag{10}$$

and the particle magnetic moment is [31]:

$$m_p = \frac{4\mu_B \pi d_p^3}{6 \times 91.25 \times 10^{-30}} \tag{11}$$

In order to quantify the MF intensity effects on the working magnetic nanofluid, a dimensionless magnetic number (Mn) can be utilized. This dimensionless value is proportional to the MF intensity and is defined as [29]:

$$Mn = \frac{\mu_0 \chi H^2 h^2}{\rho \alpha^2} \tag{12}$$

where $\mu0$, h, χ, ρ, and α are magnetic permeability in vacuum, tube hydraulic diameter, magnetic susceptibility and density of the nanofluid, and thermal diffusivity (1.599×10^{-7} m^2/s).

The k-ε RNG turbulence method is applied in this study [28], [32]:

$$\nabla \cdot \left(\rho_{ff} \vec{v}_{ff} k\right) = \nabla \cdot \left[\left(\mu + \frac{\mu_t}{\sigma_k}\right)\nabla k\right] + G_k - \rho_{ff}\varepsilon \tag{13}$$

$$\nabla \cdot \left(\rho_{ff} \vec{v}_{ff} \varepsilon\right) = \nabla \cdot \left[\left(\mu + \frac{\mu_t}{\sigma_\varepsilon}\right)\nabla \varepsilon\right] + C_{1\varepsilon}(\varepsilon / k)G_k - \frac{C_{2\varepsilon}\rho_{ff}\varepsilon^2}{k} \tag{14}$$

where k is turbulent kinetic energy, ε is dissipation rate, G_k is the generation of turbulence kinetic energy, σ_k and σ_ε are the turbulent Prandtl numbers for k and ε, respectively, $C_{1\varepsilon}$ and $C_{2\varepsilon}$ are two constants, and μ_t is the turbulent viscosity. The constants for the k-ε RNG model are defined by [33]:

$$\mu_t = \rho_{ff} C_\mu \frac{k^2}{\varepsilon}, \ C_\mu = 0.0845$$
$$C_{1\varepsilon} = 1.42, \ C_{2\varepsilon} = 1.68$$
$$\sigma_k = 1, \ \sigma_\varepsilon = 1.3 \tag{15}$$
$$G_k = 2\mu_t E_{ij} E_{ij}, \ E_{ij} = \frac{1}{2}\left(\frac{\partial u_i}{\partial x_j} + \frac{\partial u_j}{\partial x_i}\right)$$

2.2. Thermal investigation

The major goal of this investigation is to appraise the heat transfer from the absorber to the heat transfer fluid. It concerns to the convection heat transfer coefficient, in which smaller magnitudes of this variable causes a higher absorber temperature resulting in higher thermal losses. PTSCs employ the direct beam solar radiation (G_b). The existing radiation upon the collector is defined by $Q_s = A_a \cdot G_b$, and the useful heat is calculated as $Q_u = \dot{m} \cdot c_p \cdot [T_{out} - T_{in}]$, in which where A_a, $\dot{m}$, T_{in}, and T_{out} are the collector aperture, mass flow rate, inlet and outlet temperatures, respectively. The convection HTC (h) can be calculated using Nusselt number. On the plus side, Nusselt number pertains on the problem geometry and flow conditions [10]. Eqs. (16-18) indicate corresponding formula for Nusselt number, Prandtl number, and friction factor [10]:

$$Nu = \frac{hD_i}{k} \tag{16}$$

$$Pr = \frac{\mu C_p}{k} \tag{17}$$

$$f = \frac{2\Delta P}{\rho_{ff} u^2}\left(\frac{D_i}{L}\right) \tag{18}$$

where ΔP, L and u are the pressure loss, length of the receiver tube and fluid velocity, respectively. In turbulent flow regime ($Re > 2300$), the Nusselt number is determined based on Colburn correlation [34] as:

$$Nu = 0.023 \cdot Re^{0.8} \cdot Pr^{0.4} \tag{19}$$

Another relationship that can be used to calculate the Nusselt number for nanofluid was proposed by Leinhard and Leinhard [35] as follows:

$$Nu = \frac{\left(\frac{f_{th}}{8}\right) \cdot Re \cdot Pr}{1 + 12.8 \cdot \sqrt{\frac{f_{th}}{8}} \cdot (Pr^{0.68} - 1)} \text{with } f_{th} = \frac{184}{Re^{0.2}} \text{ for turbulent flow} \tag{20}$$

Petukhov relation [36] is a widely used theoretical way to calculate the friction factor using Reynolds number, as:

$$f = (0.79 \cdot \ln Re - 1.64)^{-2} \tag{21}$$

2.3. Ferrofluid Physical Properties

Ferrofluid physical properties are calculating by considering the attributes of based fluid (bf) and nanoparticles simultaneously and are presented by [24], [37], [38]:

$$\rho_{ff} = (1 - \varphi)\rho_{bf} + \varphi\rho_p \tag{22a}$$

$$C_{p,ff} = (1 - \varphi)C_{p,bf} + \varphi C_{p,p} \tag{22b}$$

$$\mu_{ff} = (1 + 2.5\varphi)\mu_{bf} \tag{22c}$$

$$k_{ff} = \left(\frac{k_p + (n-1)k_{bf} - (n-1)\varphi(k_{bf} - k_p)}{k_p + (n-1)k_{bf} + \varphi(k_{bf} - k_p)}\right)k_{bf} \tag{22d}$$

where φ and n are the volumetric fraction of the nanoparticles and shape factor, respectively. Equation (22d) was developed by Hamilton & Crossor [39]. Therminol 66 and two different nanoparticles (Fe_3O_4 and CuO) are used to form different ferrofluids for this study, with the different φ values. This volumetric fraction typically varies between 0.1 – 4%. Table 1 epitomizes the physical attributes of the whole heat transfer fluids and nanoparticles.

Table 1. Physical attributes of all heat transfer fluids and nanoparticles [29], [40]

Material		$\rho\ (kg/m^3)$	$C_p\ (J/kg.K)$	$k\ (W/m.K)$	$\mu\ (kg/m.s)$
Therminol 66 (bf)		899.5	2122	0.107	0.00106
Fe_3O_4 (p)		5200	670	6	---
CuO (p)		6500	540	18	---
Therminol 66 – Fe_3O_4 (ff)	φ = 2%	985.5	2092.96	0.113206	0.001113
	φ = 4%	1071.5	2063.92	0.119657	0.001166
Therminol 66 – CuO (ff)	φ = 2%	1011.51	2090.36	0.113431	0.001113
	φ = 4%	1123.52	2058.72	0.120125	0.001166

3. Results and Discussion

ANSYS® Fluent® version 19.1 is adopted to solve the governing equations of a three-dimensional steady-state model. As it was explained in the previous section, the turbulent model adopted here is k-ε RNG model in order to model the PTSC problem [28]. The solution of momentum and energy equations are obtained using the second order upwind differencing scheme. A convergence limit of 10^{-3} and 10^{-6} are considered for momentum, mass and energy equations. A user-defined function code is written to include the ferrofluid properties and MF in all the simulations.

The flowing fluid possesses uniform velocity and temperature at the tube inlet as $u = u_0, T_f = T_0 = 230$ ℃. As it was stated before, an outer surface of the tube receives a uniform heat flux due to the solar reflection from the collector (taking into account the mirror efficiency), while top surface receives direct solar radiation for the sun. Therefore, top and bottom half tube surfaces are subjected to $\dot{q}_{up} = I_g$ and $\dot{q}_{down} = I_b C_R$, respectively, in which I_g is global radiation with the intensity of 680 W/m^2, I_b is beam radiation with the intensity of 630 W/m^2, and C_R is about 15.46. Also, outlet boundary condition is assumed to be zero pressure gradient. In addition, it is assumed that nanoparticles have spherical shape with a diameter of 10 – 20 nm, and hence the shape factor (n) would be equal to 3 [29]. The Biot–Savart law is applied to compute the MF produced by current-carrying wire as:

$$B = \frac{\mu_0 I}{2\pi r} \tag{23}$$

where, r is the distance between MF calculation point and the wire location.

The discretized model for the current work is composed by hexahedral cells in all regions (fluid and receiver tube). The boundary layer between the receiver tube inner wall and the working fluid was defined in such a way to have a good output for the y+ parameter, which can be calculated as [41]:

$$y+ \equiv \frac{u^* \cdot y}{v} \tag{24}$$

in which u^*, y, and v are defined as friction velocity at the nearest wall, distance to the nearest wall, and local kinematic viscosity of the fluid, respectively. A value close to 1 can be considered as a good output for the y+, and hence, the discretized model can capture near wall boundary layer adequately [42]–[44]. A mesh sensitivity analysis was made for the receiver tube and thermal efficiency of solar collector as well as y+ of receiver tube were calculated for different meshes. Table 2 gives the results of the mesh sensitivity analysis, in which it was performed for the smooth absorber and for inlet temperature equal to 230°C. Finally and according to these results, a mesh with around twelve million cells (very fine case) was selected as a good discretization model for current problem. A schematic of the discretized model with the very fine mesh case was shown in Figure 1(d).

Table 2. Mesh discretization effect on the thermal efficiency and y+ parameter of the solar collector

Mesh type	Coarse	Medium	Fine	Very fine
# of cells	2,909,300	5,753,248	8,461,704	12,022,300
y+	2.1	1.6	1.25	1.15
$\boldsymbol{\eta_{th}}$	0.7195	0.7258	0.7295	0.7305

Variation of Nusselt number obtained from the current simulation for *smooth tube* with all the working fluids with nanoparticle size of 10 nm, and those obtained using either Eqs. (19) and (20) are used to validate the numerical model. Equation (19) is used to validate the base fluid, while Eq. (20) is used to validate the ferrofluids, according to [27], [45]. Figure 3 presents the outputs of the validity study, in which the current CFD outputs are in accordance with the results from theory, leading to have less than 6% error between them. In all the graphs in this section, the curve names consist of the following parts: CuO or Fe_3O_4 which refers to the type of nanoparticles, 2% or 4% refers to the volumetric fraction of the particles, B refers to the intensity of the MF, and 10 nm or 20 nm refers to the size of nanoparticles. When needed, a magnification was added to some figures to better understand the comparison between different cases.

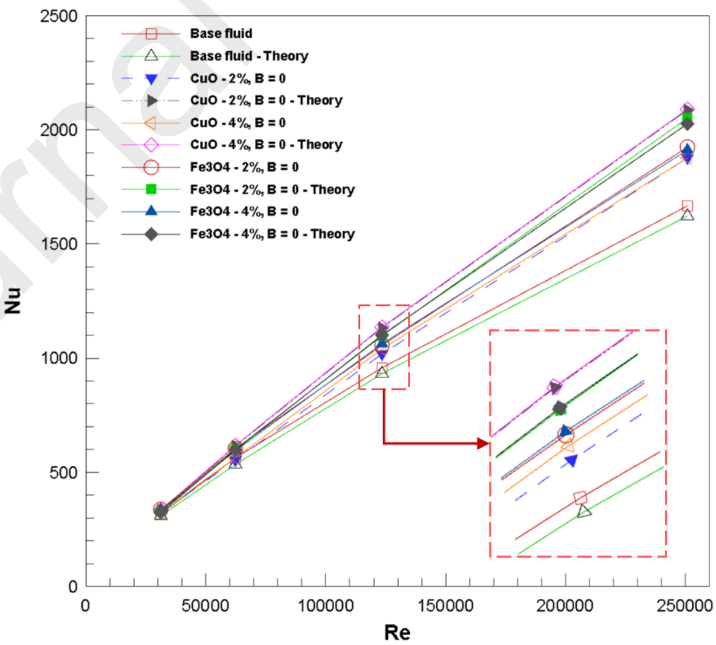

Fig 3. Nusselt number variation for the current model and from the theories.

3.1. Simulation Results for Smooth Tube

Ferrofluids with different volume fractions (2% and 4%) are used as the working fluid for the PTSC. As above mentioned, the MF investigated in the research, was generated through a wire placed near to the receiver tube. MF effects on the local HTC for nanoparticles of 10nm and 20nm are shown in Figure 4. The figure reveals that the HTC has a tendency to increase with a growth in Reynolds number for all working fluids, and also nanoparticles help to possess higher HTC compared to the base fluid. In addition, the HTC shows an increasing behavior for higher values of φ, as clearly can be seen in Figure 4b and 4c, which is mainly due to have more nanoparticles in the ferrofluid, and hence, higher thermal conductivity for the ferrofluid. Furthermore, it was observed that the applied MF enhances the cooling performance of the ferrofluid. Furthermore, the 4% Fe_3O_4/Therminol 66 ferrofluid with 10nm particles size and with the MF showed the highest convective HTC. The HTC of ferrofluid and particle size have an inverse relation (one decreases, the other increases).

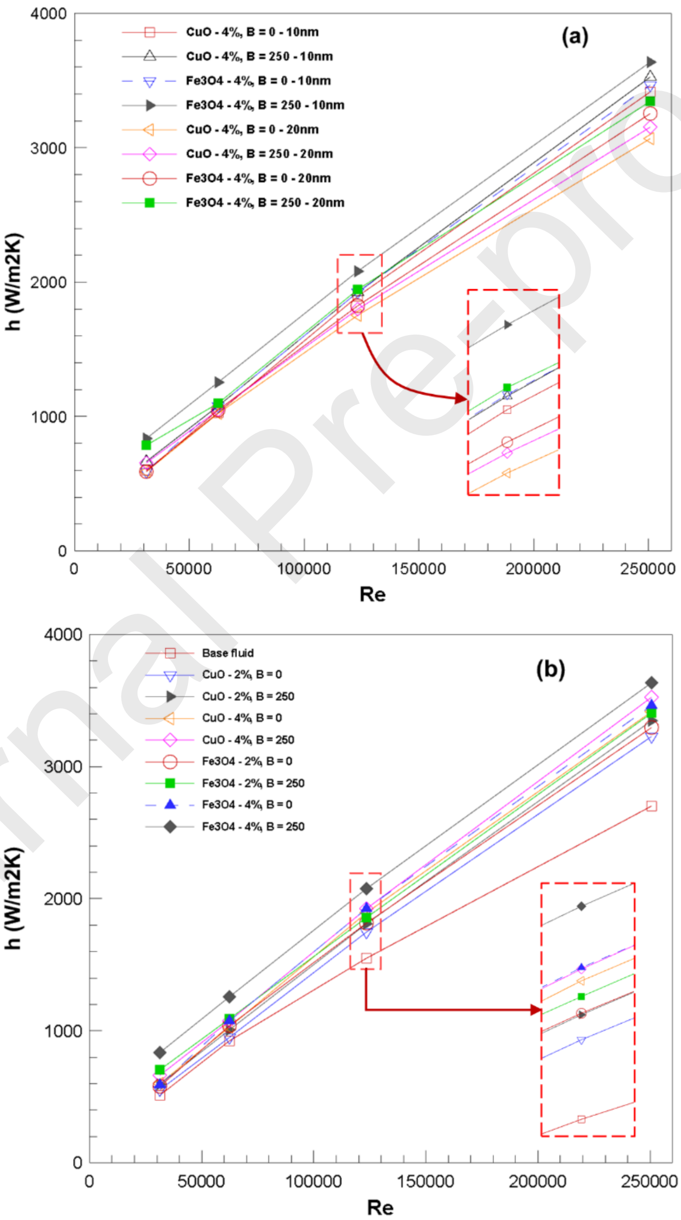

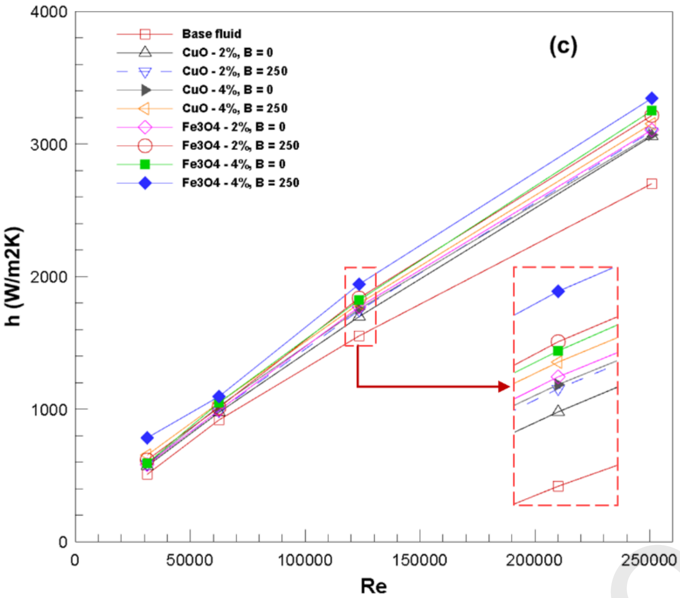

Fig. 4. Local convective HTC (h): (a) comparison between two particle sizes, (b) particle size of 10nm, and (c) particle size of 20nm.

The gradient of velocity close to the walls is enhanced mainly because of the presence of non-uniform transverse MF. This results in increasing the HTC value, as it was shown in Figure 4. Figure 5 shows contour of temperature and velocity for the base fluid at the outlet, considering the inlet temperature of 503 K and Re of 31000 and 62000, respectively. In addition, Figures 6 illustrate outlet velocity for T_{in} = 503 K, $B = 0\ G$, and $250\ G$, and Re_{ff} $= 31000$, and for particle size of 10nm for both CuO and Fe_3O_4 ferrofluids. This figure demonstrates the enhancement in velocity in the case of ferrofluid with the MF. Also, Fe_3O_4 ferrofluid shows better performance than CuO in terms of velocity distribution at the outlet, comparing Figure 6a and 6c with Figure 6b and 6d.

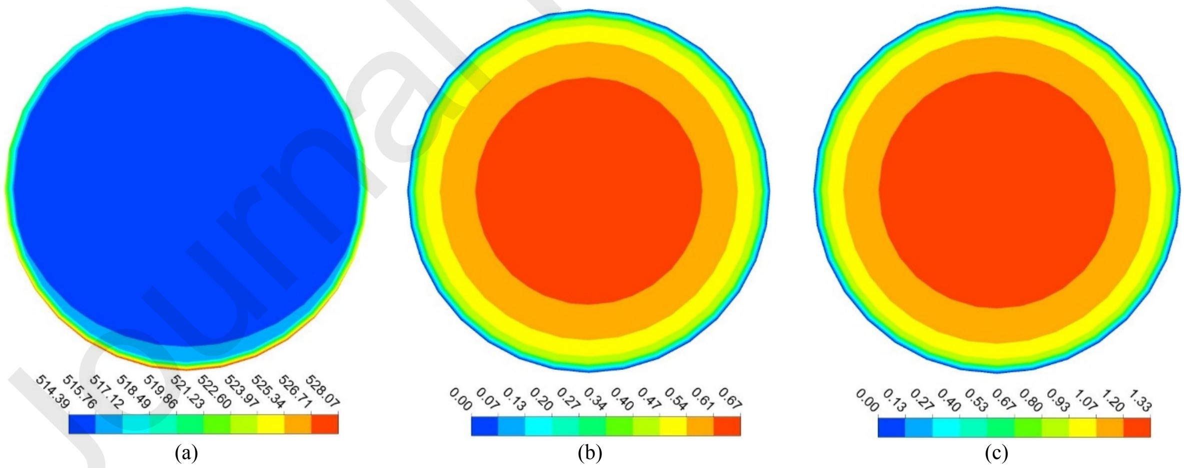

Fig 5. Results for the base fluid for T_{in} = 503 K: (a) outlet temperature (K) for Re = 31000, and velocities (m/s) for: (b) Re = 31000 and (c) Re = 62000.

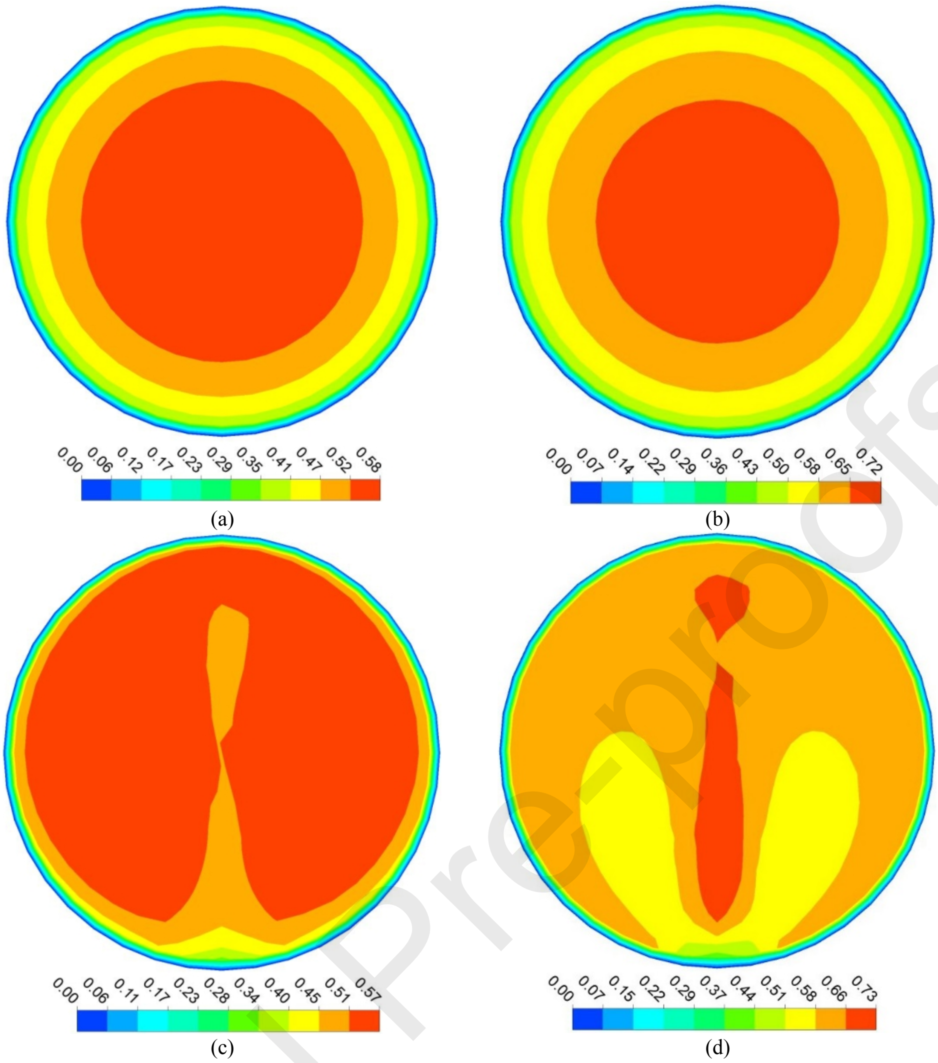

Fig 6. Outlet velocity (m/s) assuming Re = 31000, T_{in} = 503 °K, φ = 4% and particle size of 10nm, for: (a) CuO with B = 0, (b) Fe_3O_4 with B = 0, (c) CuO with B = 250G, and (d) Fe_3O_4 with B = 250G.

Figure 7 shows the temperature distributions at the outlet for both ferrofluids with volume fraction of 4%, Re of 31000, T_{in} equal to 503K, particle size of 10nm, and MF of 0 and 250G. Though surface temperature of the receiver tube for $B = 0$ reaches a higher value than $B = 250$, MF forces the majority of fluid to flow with the maximum temperature. In addition, maximum temperature of CuO ferrofluid is bigger than Fe_3O_4, for both MFs of 0 and 250G. However, larger portion of the Fe_3O_4 case reach a bigger temperature value, see minimum temperature of all cases from Figure 8.

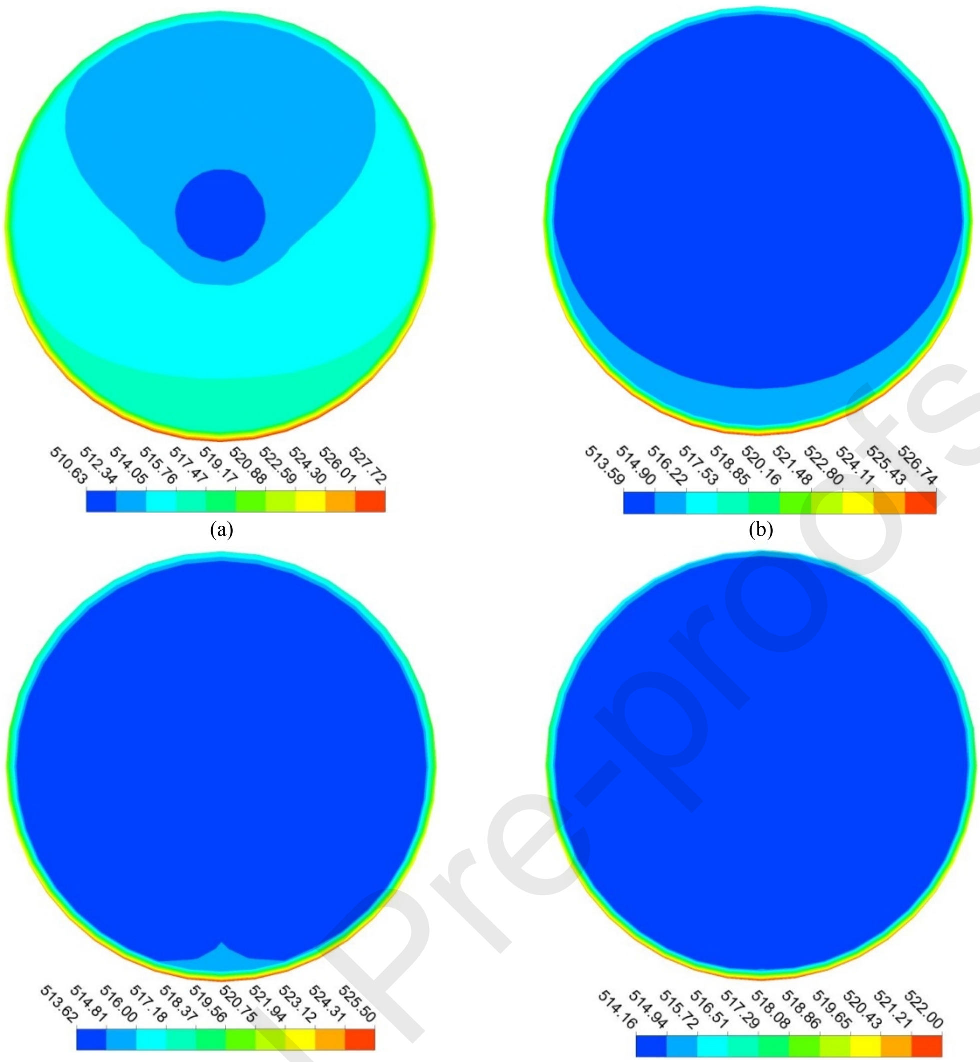

(d) (e)

Fig 7. Outlet temperature (K) for ferrofluids with Re = 31000, T_{in} = 503 °K, φ = 4% and particle size of 10nm, for: (a) CuO with B = 0, (b) Fe_3O_4 with B = 0, (c) CuO with B = 250G, and (d) Fe_3O_4 with B = 250G.

Figure 8 presents the variation of Nusselt number in the presence of MF and for two different nanoparticle sizes. Similar to the HTC variation from Figure 4, smaller particle size improves better the variation of the Nusselt number than bigger particle sizes, by comparison between Figures 8a and 8b. Nusselt number grows with Reynolds number for all working fluids, while ferrofluid experiences higher values compared to the base fluid. As it was stated before, incorporating nanoparticles within ferrofluids led to have higher thermal conductivity, mainly due to the high conductivity of nanoparticles. Therefore, HTC of the ferrofluid are increased more than base fluid. Higher φ values lead to have bigger effective thermal conductivity for ferrofluid, and hence, higher Nusselt number.

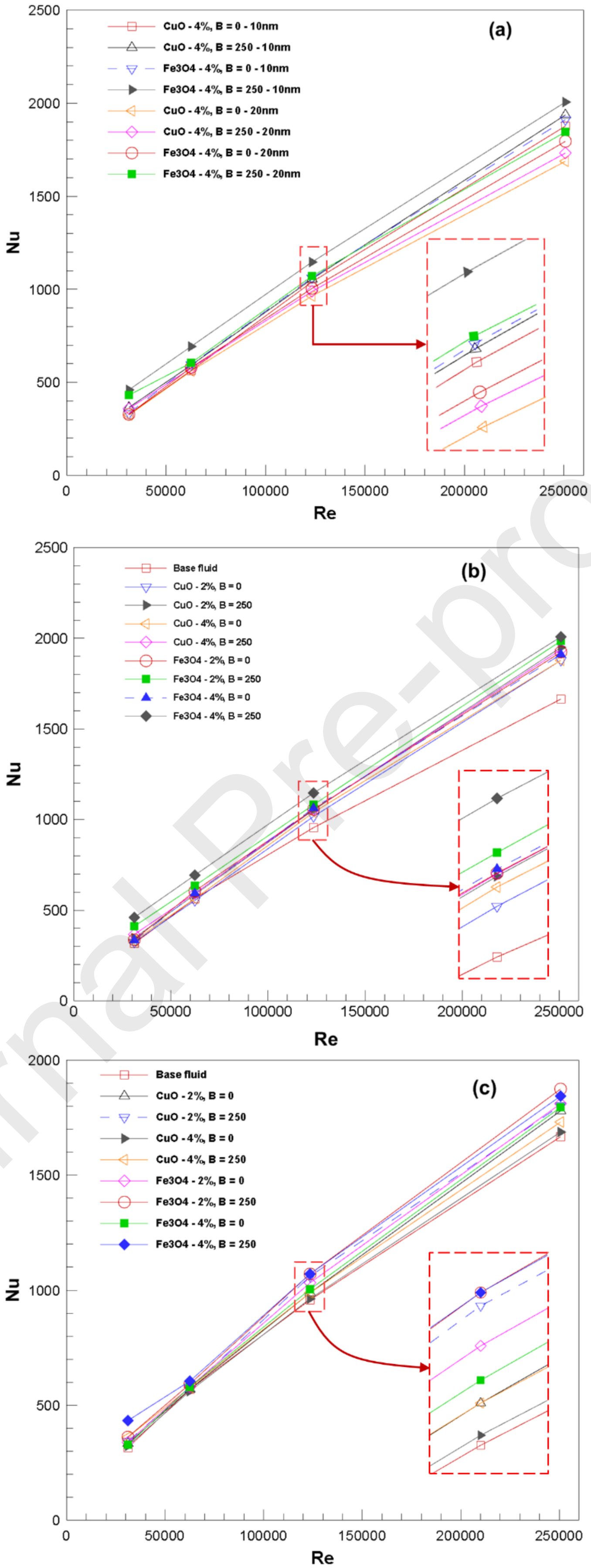

Fig. 8. Effects of MF on the Nusselt number: (a) comparison between two particle sizes, (b) particle size of 10nm, and (c) particle size of 20nm.

Friction factor variation for both CuO and Fe_3O_4 ferrofluids are shown in Figure 9, with and without attendance of MF, different volume fractions and particle sizes. Higher density and viscosity for ferrofluids result in higher friction factor than the base fluid. In addition, the highest friction factor from all cases is for Fe_3O_4 ferrofluid with 20nm particle size and 250G MF; see Figure 9a. Figures 9b and 9c show the friction factor for particle size of 10nm and 20nm, respectively. More importantly, friction factor increases in the attendance of MF, according to Figure 9.

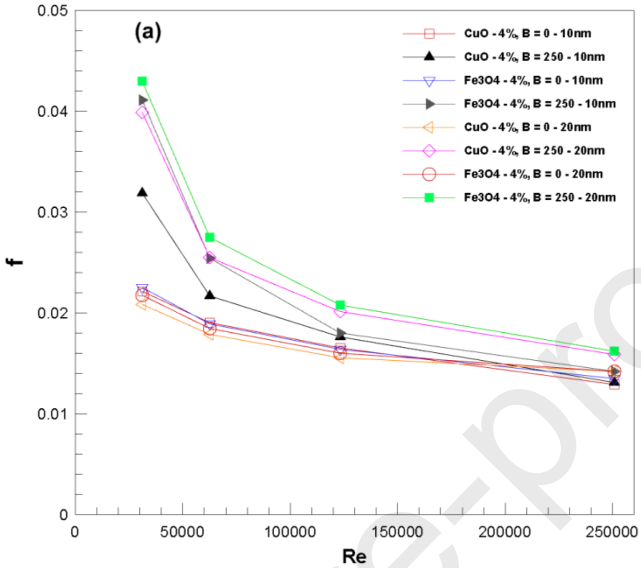

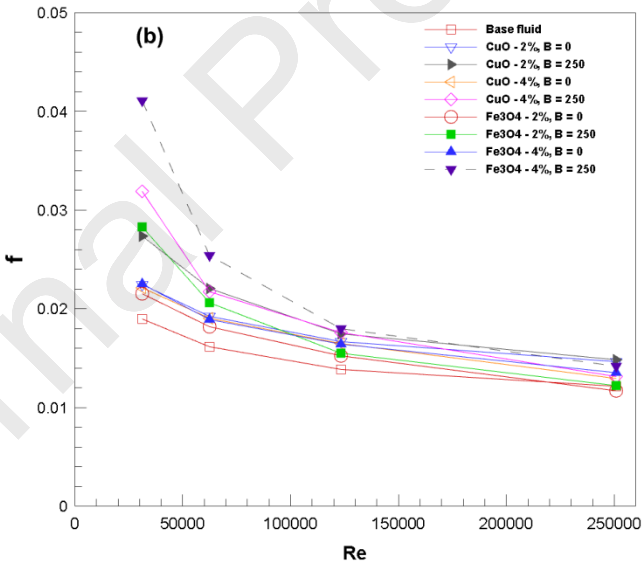

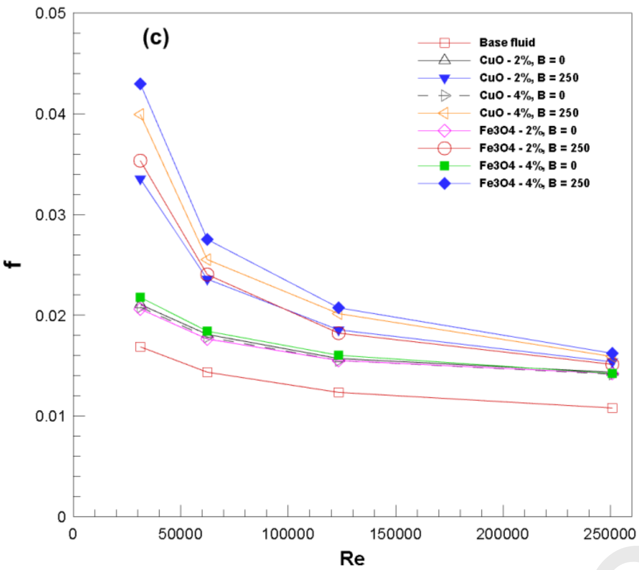

Fig. 9. Variation of the friction factor (f) in the presence of MFs: (a) comparison between two particle sizes, (b) particle size of 10nm, and (c) particle size of 20nm.

According to the results presented in Figure 9, friction factor drops with the higher values of Reynolds number. As it was presented in Eq. (18), there is an inverse relationship between friction factor and velocity. Velocity streamlines at the receiver tube outlet are presented in Figure 10, for B = 0 and 250G, $Re_{ff} = 31000$, φ = 4%, and particle size of 10 nm. It could be noticed that the MF forces the boundary layers to move to the tube central parts, similar to the distribution of outlet temperature. As can be observed from Fig. 10c and 10d, force generated by the MF in the transverse plane produces secondary flows and two vortices. This force can be augmented by enhancing the intensities of MF. On the other hand, the maximum outlet velocity for $B = 0$ is concentrated at the tube central part, see Figure 10a and 10b. Due to the presence of MFs, ferrofluid particles are more concentrated near the tube bottom side, which clarifies why there are vortices in Fig. 10c and 10d, and no vortices in Fig. 10a and 10b.

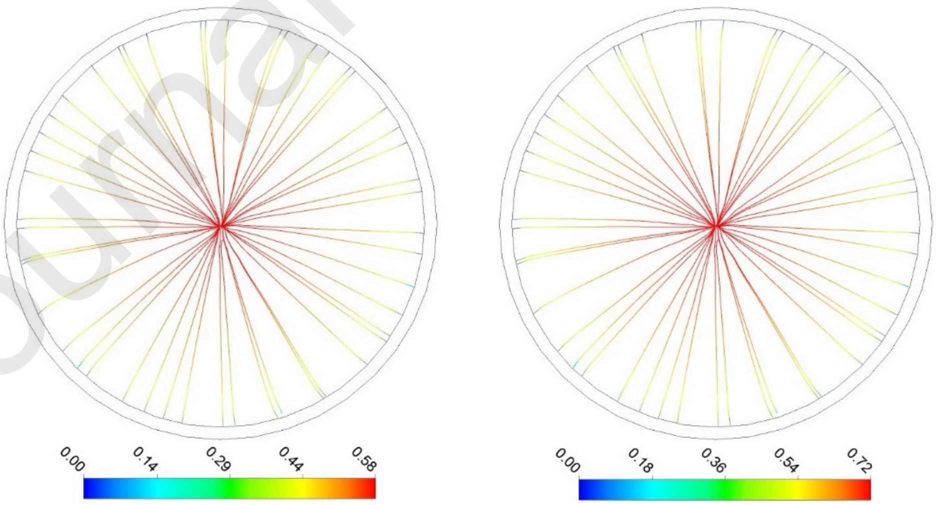

(a) (b)

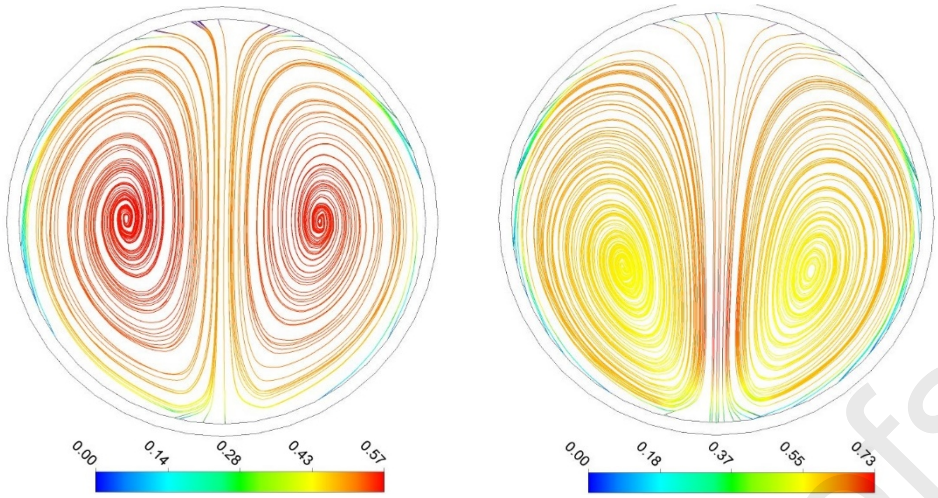

(c) (d)

Fig 10. Outlet velocity streamline (in m/s) for Re = 31000, T_{in} = 503 °K, φ = 4% and particle size of 10nm, for: (a) CuO with B = 0, (b) Fe_3O_4 with B = 0, (c) CuO with B = 250G, and (d) Fe_3O_4 with B = 250G.

Performance evaluation criteria (PEC) has been introduced as a proven approach to appraise the thermo-hydraulic manner of flowing working fluid in the receiver tube [46], which is calculated by:

$$PEC = \frac{Nu/Nu_0}{(f/f_0)^{1/3}} \tag{25}$$

in which Nu_0, f_0, f and Nu are the Nusselt number and friction factor of the receiver tube working with base fluid and ferrofluid, respectively. Accordingly, for an effective approach the PEC value is greater than one, which means a better performance from thermo-hydraulic point of view. PEC variation for both ferrofluids with volume fractions of 2 and 4%, both particle sizes, and different MF intensities, is shown in Fig. 11. As it can be seen from these two figures, Fe_3O_4/Therminol 66 with φ = 4% and B = 250 shows the best thermo-hydraulic performance. As it was explained before, MF leads to a bigger HTC and friction factor. In addition, the enhancements in HTCs are bigger than friction factors, and as result, the PEC for ferrofluids with B = 250 show an increasing behavior.

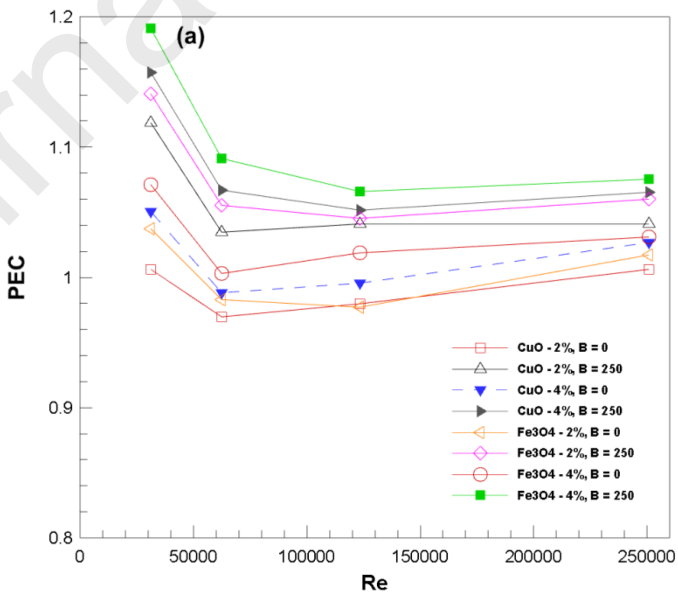

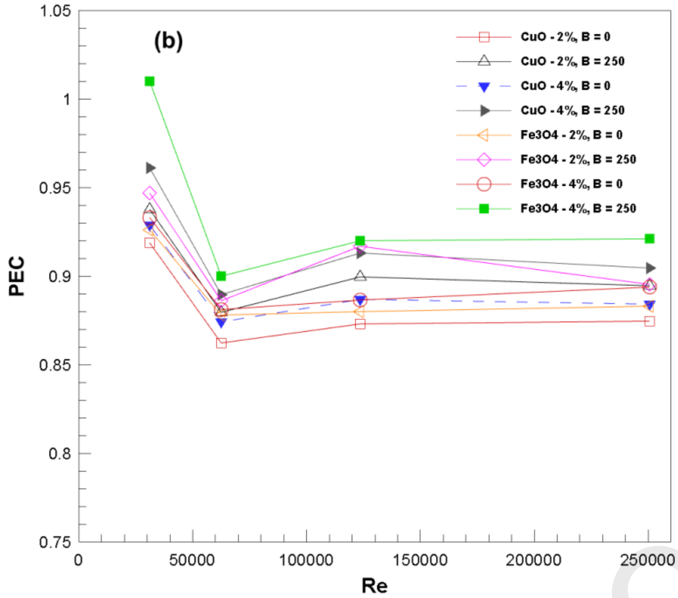

Fig. 11. Variation of PEC in the presence of MF, for: (a) particle size of 10nm, and (b) particle size of 20nm.

The receiver thermal loss can be calculated using the following relation [27]:

$$Q_{loss} = Q_{abs} - Q_u \tag{26}$$

where Q_{abs} is defined as the absorbed solar energy and can be estimated as follows [27]:

$$Q_{abs} = Q_s \cdot \eta_{\text{opt,max}} \cdot K(\theta) \tag{27}$$

in which $\eta_{\text{opt,max}}$ is the maximum optical efficiency and for current work is equal to 75.5%, and $K(\theta)$ is the incident angle modifier. This last parameter depends on the incident angle on the collector aperture (θ) and for the present study is considered equal to 1 since the PTS collector is surveyed for zero incident angle. Figure 12 present the receiver thermal loss variation versus Reynolds number for all the cases with smooth receiver tube, utilizing the Eq. (26). As it was expected, the thermal loss for the PTSC with the base fluid is bigger than all the other cases, and lower heat loss was obtained with Fe_3O_4/Therminol 66 ferrofluid of 4% volumetric fraction and with MF intensities of 250 G.

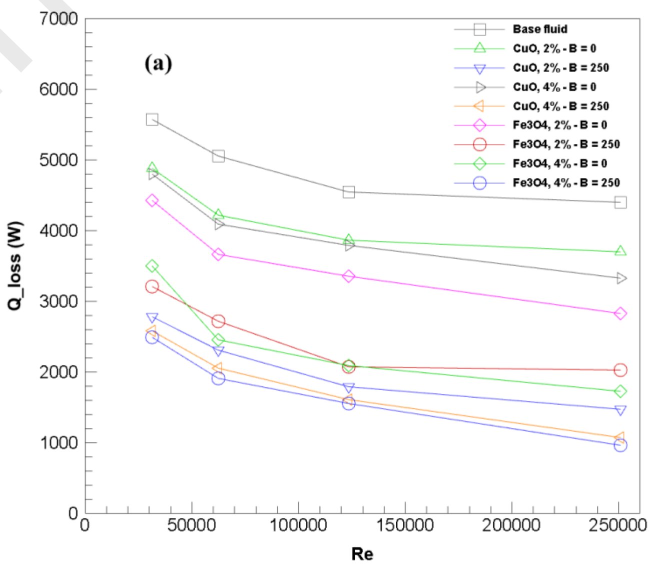

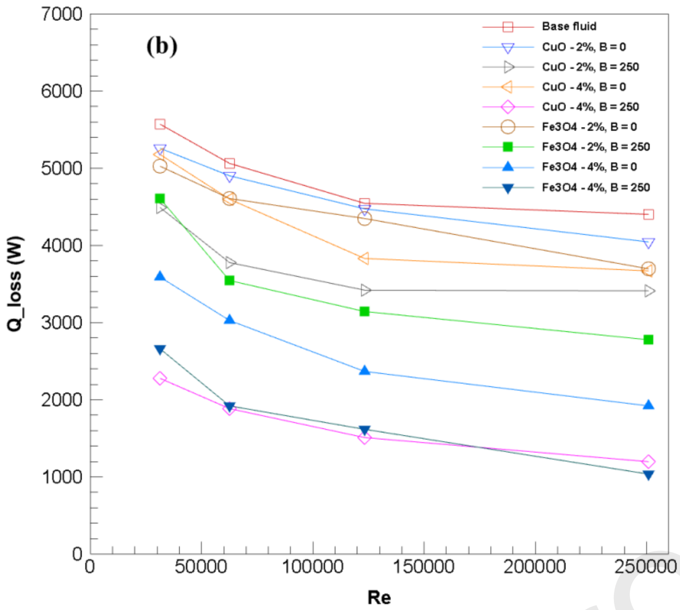

Fig. 12. Variation of heat loss in the presence of MF, for: (a) particle size of 10nm, and (b) particle size of 20nm.

The thermal efficiency of the solar collector is defined using the following equation [27]:

$$\eta_{th} = \frac{Q_u}{Q_s} \tag{28}$$

The main parameter to evaluate the solar collector is its thermal efficiency. Variation of thermal efficiency for all working fluids, with different φ and B values, and with particle size of 10nm and 20nm is presented in Figure 13. MF helps to have higher thermal efficiency for the collector. As it was stated before, the bigger values of φ lead to have higher thermal conductivity for the ferrofluids, and according to Figure 13 this leads to an increase in the efficiency. Therefore, more SE can be absorbed by the receiver tube with ferrofluids, and hence resulting in more thermal energy conversion. Korres et al. [14] have reported that the thermal efficiency of a PTSC with Syltherm 800/CuO nanofluid showed an average of 1.24% enhancement compared to Syltherm 800 case. According to Figure 14, the average of enhancement in the thermal efficiency for CuO/Therminol 66 is around 1.35% for $B = 0$ and around 4.0% for $B = 250\,G$.

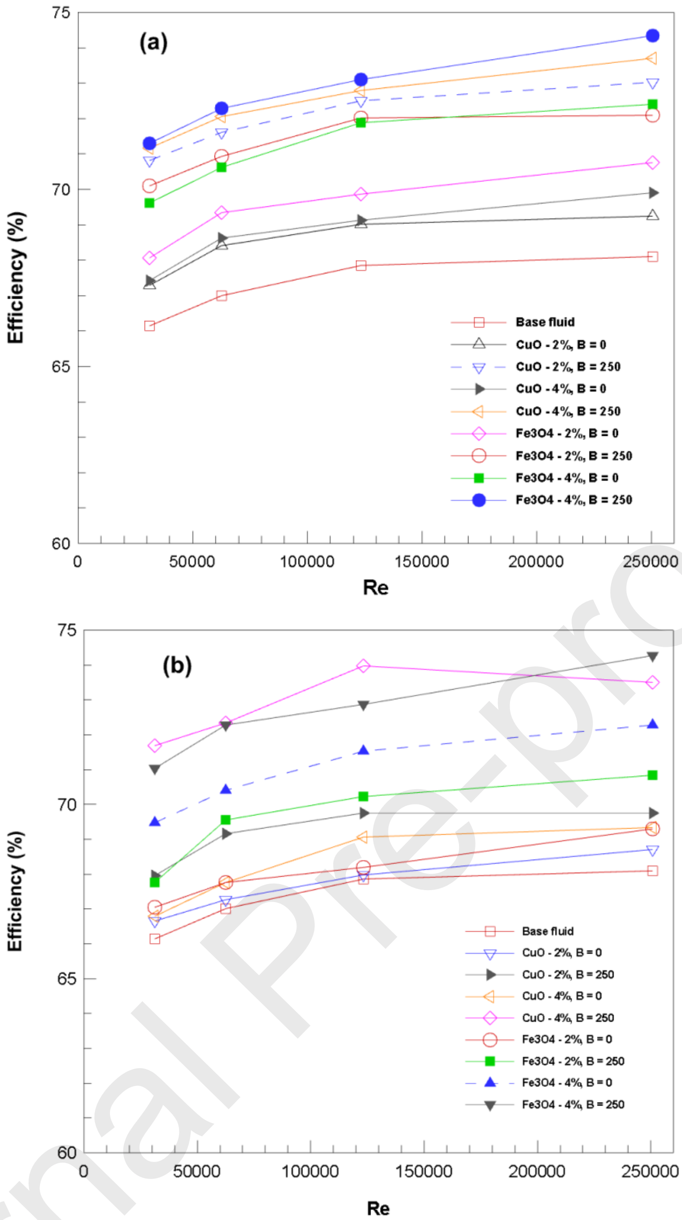

Fig. 13. Thermal efficiency for all working fluids: (a) particle size of 10nm, and (b) particle size of 20nm.

3.2. Results for Finned Tube

According to Bellos et al. [47] and Olia et al. [48], incorporating fins within collector tube can enhance the performances of the PTC system. Four fins with the length of 10 mm were utilized for the finned receiver tube, as shown in Figure 1c. In addition, as it was discussed in section 3.1, nanoparticle size of 10nm show better performance than the 20nm particle size. Also, Fe_3O_4/Therminol 66 ferrofluid delivered better performance than the CuO/Therminol 66, and of course with larger volume fraction, i.e., 4%. Therefore, Fe_3O_4/Therminol 66 ferrofluid with φ = 4% and particle size of 10nm are considered for the finned tube, to analyze the effect of MF along with the fins on the performance of the PTC system.

Figure 14 presents variation of heat transfer coefficient, Nusselt number, friction factor, and performance evaluation criteria for finned tube with and without presence of MFs and for base and Fe_3O_4 nanofluid with 4% volume fraction of 10nm particle size. As can be seen from this figure, finned tube shows a better performance in terms of all these parameters, where the best enhancement behavior is for the finned tube with Fe_3O_4/Therminol 66 working fluid and in the presence of MF.

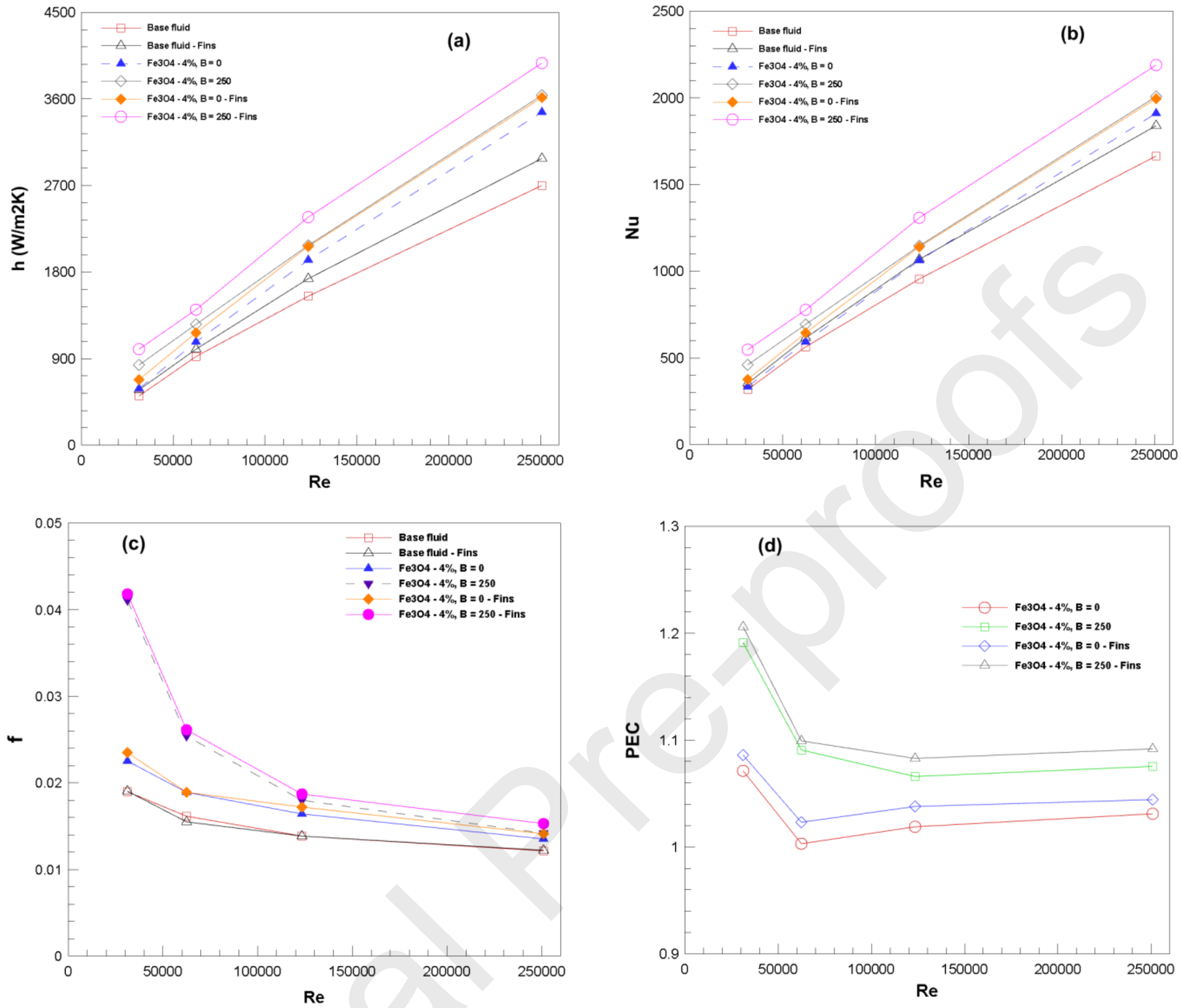

Fig. 14. MF and fins effects on the: (a) HTC, (b) Nusselt number, (c) friction factor, and (d) PEC, for nanoparticle size of 10nm.

Figure 15 presents distribution of the outlet temperature and outlet velocity streamline for finned tube with base fluid and Fe_3O_4/Therminol 66 ferrofluid (4% volume fraction). Particle size is 10nm, Reynolds number is 30000 and MF is 250G. The effects of fins to increase the outlet temperature are clarified by comparing Fig. 15a with 5a and 15b with 7d, with average outlet temperatures of 513.85, 514.25, 514.41, and 514.56, respectively. In addition, velocity streamline magnitudes and configurations are affected by the presence of fins, comparing Fig. 15d with Fig. 10d. Figure 15c is used to compare the base fluid velocity distribution with ferrofluid distribution in the presence of fins and MF.

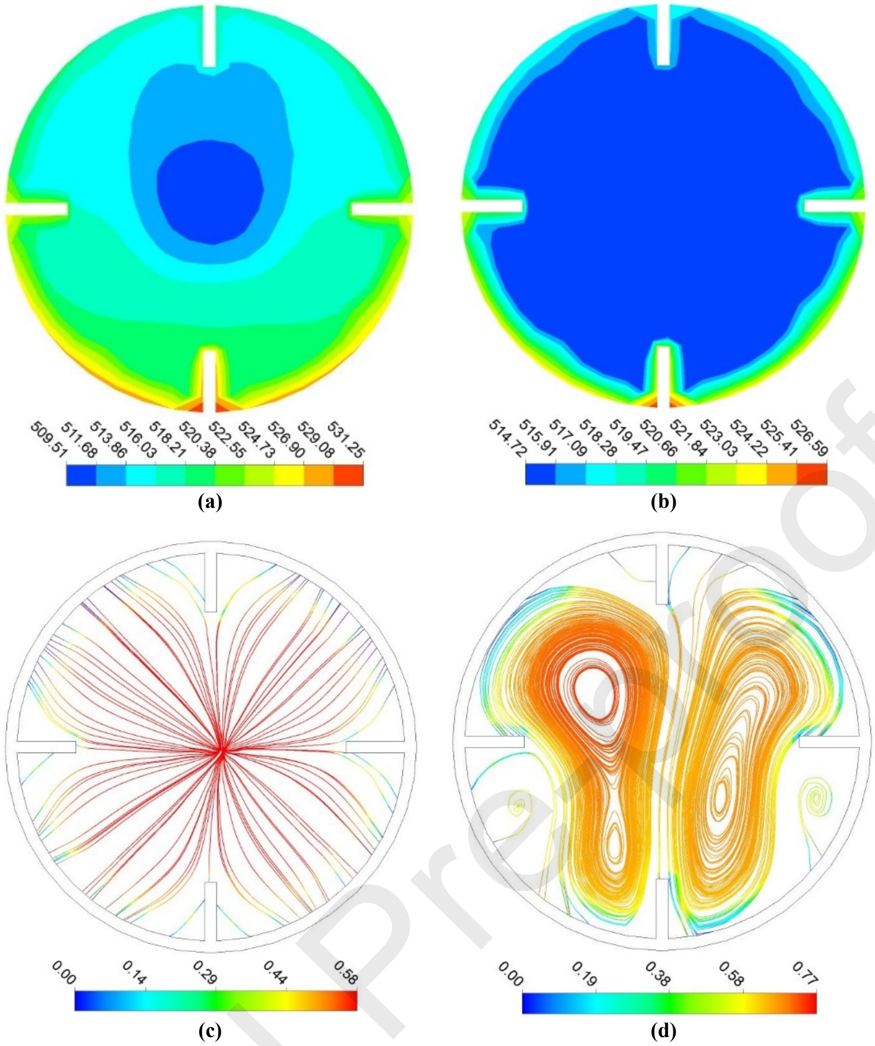

Fig. 15. (a) and (b) outlet temperature (K) for base fluid and Fe_3O_4 with B = 250G, (c) and (d) outlet velocity streamline (in m/s) for base fluid and Fe_3O_4 with B = 250G. Other parameters are: Re = 31000, T_{in} = 503 °K, φ = 4% and particle size of 10nm, for finned tube.

Similar to PTC with smooth tube, the heat loss of the PTC with finned tube along with corresponding results for the smooth tube are shown in Figure 16. As can be seen from this figure, the PTC with finned tube delivered the lower heat loss compared with the smooth receiver tube. In addition and similar to the previous findings, the presence of MFs helped to have even lower hear loss in comparison to PTC without the presence of MFs.

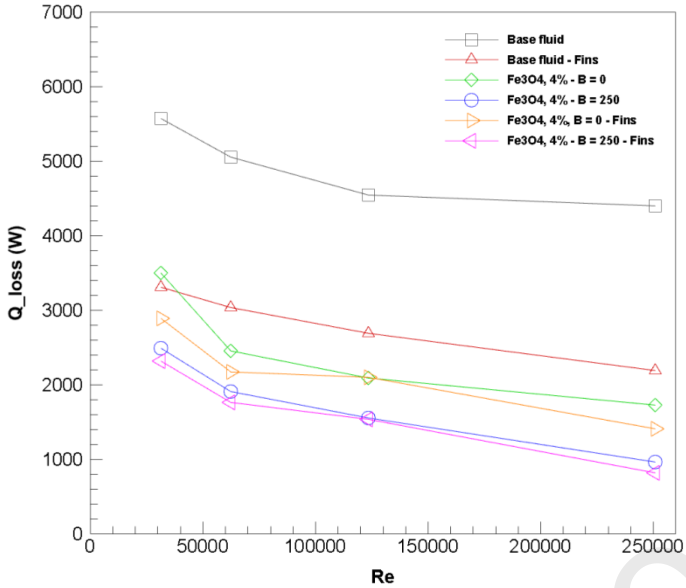

Fig. 16. Heat loss of the solar collector with smooth and finned tubes, for base and Fe3O4/Therminol 66 fluids. Particle size is 10nm, and MFs are B = 0 and 250.

As a result of enhancing outlet temperature due to the presence of fins, the solar collector efficiency is also increases as presented in Fig. 17. This figure is also for the base fluid and Fe_3O_4 ferrofluid with particle size of 10nm. MF intensities are 0 and 250G and volume fraction of nanoparticles are 4%. As can be seen from this figure, finned receiver tube with ferrofluid in the presence of MF delivers the highest efficiency compared to the other cases.

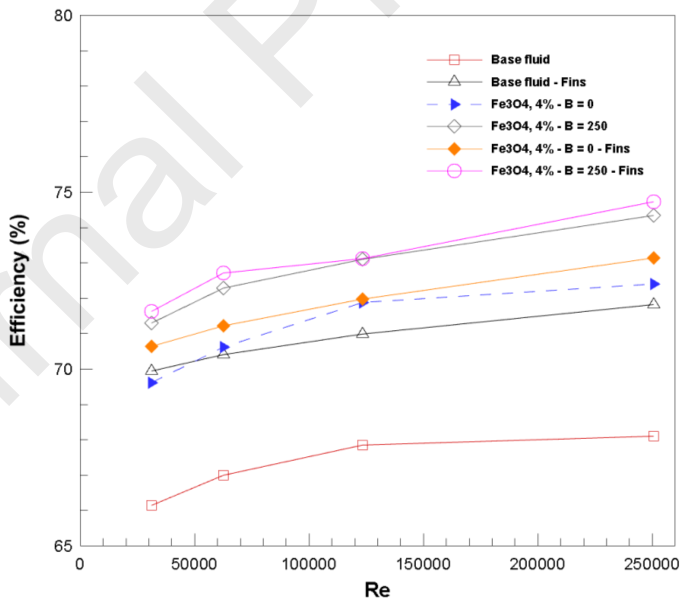

Fig. 17. Thermal efficiency of the solar collector with smooth and finned tubes, for base and Fe3O4/Therminol 66 fluids. Particle size is 10nm, and MFs are B = 0 and 250.

Another important parameter to be examined is the financial assessment of the collector with smooth and finned tubes. To do this, the levelized cost of energy (LCOE) was proven to be the best approach [28], [49]. According to Conrado et al. [49], the PTC cost with smooth receiver tube is about 200 Euros/m^2, while cost of the finned tube is about 3% higher [28]. Current PTC collector has 85 m^2 aperture, and hence, the cost of PTC with smooth and finned tubes is around 17,000 and 17,510 Euros, respectively. Following equation can be used to calculate the LCOE [47]:

$$LCOE = \frac{CO}{Q_u\,N} = \frac{CO}{\eta_{th}\,Q_s\,N} \tag{29}$$

in which N is the system total operation hours. This parameter is calculated for all the operating PTC lifetime. Considering the typical lifetime of mechanical equipments, parameter N for the current study is considered to be around 24000 hours (total life of 20 years, with 1200 h per year). The reader should note that the LCOE estimates presented here are only cost indications of the PTC collector part with the working fluids studied here, not for the whole solar power plant.

Figure 18 presents the LCOE variation with Reynolds number for the current PTC with smooth and finned tubes, and for different working fluids. According to Bellos et al. [47], the LCOE for smooth and finned tubes are almost the same for inlet temperature of 493 – 503 K, as can be seen in Fig. 18a. While LCOE would be larger for finned tube that smooth one for lower inlet temperatures. Therefore, PTC with smooth tube must be selected for low inlet temperatures, while for higher inlet temperatures than (higher than 503 K) the finned tube must be selected.

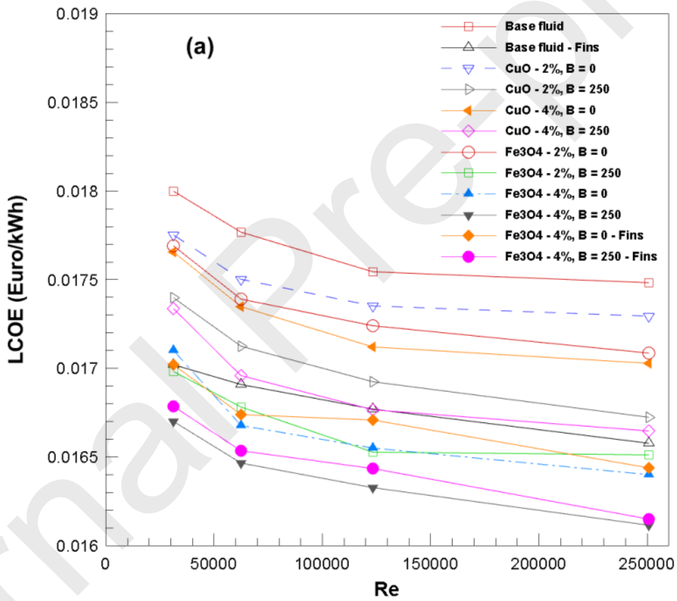

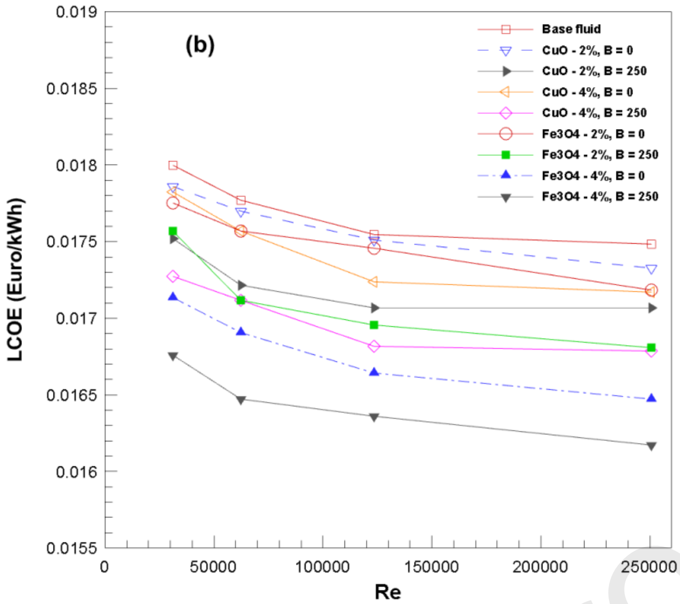

Fig. 18. LCOE for collector with smooth and finned tubes, for different working fluids and MFs are B = 0 and 250, and for: (a) particle size of 10nm, and (b) particle size of 20nm.

4. Conclusions

In the current research, a numerical simulation was exerted for the comparison between CuO/Therminol 66 and Fe_3O_4/Therminol 66 at the presence of MF, which were proposed as working fluid for a parabolic trough solar collector (PTSC). This comparison was done using CFD approach. Besides, the central receiver was designed with internal fins and the distribution of the thermal and fluid flow characteristics of the ferrofluids impressed by MF for the finned tube and smooth tube were compared and evaluated. The influence of MF and particle size of nanoparticles over the collector efficiency were analyzed and discussed. The following results were drawn from the current study:

- Enhancing Reynolds number rises the convective heat transfer coefficient (CHTC) for the base fluid and ferrofluids.
- When the volume fraction and particle size of nanoparticles enhance, the CHTC augments as well.The maximum CHTC belongs to 4% Fe_3O_4/Therminol 66 with the particle size of 10 nm and in the presence of MF. Rising the particle size decreases the CHTC. The same outcomes were obtained for the Nusselt number.
- Investigation of the friction factor for the ferrofluids and base fluid demonstrated that the friction factor of the ferrofluids is higher than the base fluid. The 4% Fe_3O_4-Therminol 66 with the particle size of 20 nm and under MF has the maximum friction factor.
- Performance evaluation criteria (PEC) was considered as an evaluation parameter for the solar collector. The analyses have shown that increasing the MF and decreasing the particle size can augment the PEC. The same consequences were obtained for the efficiency of the collector. The solar collector working with 4% Fe_3O_4-Therminol 66 under MF with the particle size of 10 nm indicates better performance compared to the base fluid as well as CuO/Therminol 66.
- Although CuO nanoparticles have a higher thermal conductivity compared to Fe_3O_4 particles, this study has shown that under magnetic field Fe_3O_4 performs better than CuO for improving the collector

efficiency. Moreover, PTC with finned tube illustrates better proficiency in terms of enhancing heat transfer characteristics from tube to the working fluids. Finally, PTCs with smooth and finned tubes and Fe_3O_4/Therminol 66 with 4% volume fraction as working fluid and in the presence of MF have almost the same levelized cost of energy, while the other cases show higher values for this parameter. The average of enhancement in the thermal efficiency for CuO/Therminol 66 is around 1.35% for $B = 0$, and around 4.0% for $B = 250\,G$, while an enhancement of 1.24% was reported by Korres et al. [14] for Syltherm 800/CuO for a PTSC with $B = 0$, i.e. no magnetic field.

Acknowledgments

The first author would like to acknowledge the financial support from the Aarhus University. The second and third authors acknowledge Aalto University for the financial support of this project.

References

[1] "Global Warming of 1.5 °C." [Online]. Available: https://www.ipcc.ch/sr15/. [Accessed: 21-Jan-2019].

[2] A. Khosravi, R. N. N. Koury, L. Machado, and J. J. G. Pabon, "Prediction of wind speed and wind direction using artificial neural network, support vector regression and adaptive neuro-fuzzy inference system," *Sustain. Energy Technol. Assessments*, vol. 25, pp. 146–160, Feb. 2018.

[3] A. Khosravi, S. Syri, M. El Haj Assad, and M. Malekan, "Thermodynamic and Economic Analysis of a Hybrid Ocean Thermal Energy Conversion/Photovoltaic System with Hydrogen-Based Energy Storage System," *Energy*, vol. 172, pp. 304–319, 2019.

[4] A. Khosravi, R. O. Nunes, M. E. H. Assad, and L. Machado, "Comparison of artificial intelligence methods in estimation of daily global solar radiation," *J. Clean. Prod.*, vol. 194, pp. 342–358, Sep. 2018.

[5] F. Ullah and M. Kang, "Impact of air flow rate on drying of apples and performance assessment of parabolic trough solar collector," *Appl. Therm. Eng.*, vol. 127, pp. 275–280, Dec. 2017.

[6] P. D. Malali, S. K. Chaturvedi, and R. Agarwala, "Effects of circumsolar radiation on the optimal performance of a Stirling heat engine coupled with a parabolic dish solar collector," *Appl. Therm. Eng.*, vol. 159, p. 113961, Aug. 2019.

[7] B. Zou, Y. Jiang, Y. Yao, and H. Yang, "Optical performance of parabolic trough solar collectors under condition of multiple optical factors," *Appl. Therm. Eng.*, vol. 160, p. 114070, Sep. 2019.

[8] F. A. Al-Sulaiman, M. I. Zubair, M. Atif, P. Gandhidasan, S. A. Al-Dini, and M. A. Antar, "Humidification dehumidification desalination system using parabolic trough solar air collector," *Appl. Therm. Eng.*, vol. 75, pp. 809–816, Jan. 2015.

[9] B. Zou, H. Yang, Y. Yao, and Y. Jiang, "A detailed study on the effects of sunshape and incident angle on the optical performance of parabolic trough solar collectors," *Appl. Therm. Eng.*, vol. 126, pp. 81–91, Nov. 2017.

[10] A. Khosravi, M. Malekan, and M. E. H. Assad, "Numerical analysis of magnetic field effects on the heat transfer enhancement in ferrofluids for a parabolic trough solar collector," *Renew. Energy*, vol. 134, pp. 54–63, Apr. 2019.

[11] S. Pavlovic, A. M. Daabo, E. Bellos, V. Stefanovic, S. Mahmoud, and R. K. Al-Dadah, "Experimental and numerical investigation on the optical and thermal performance of solar parabolic dish and corrugated spiral cavity receiver," *J. Clean. Prod.*, vol. 150, pp. 75–92, May 2017.

[12] P. D. Tagle-Salazar, K. D. P. Nigam, and C. I. Rivera-Solorio, "Heat transfer model for thermal performance analysis of parabolic trough solar collectors using nanofluids," *Renew. Energy*, vol. 125, pp. 334–343, Sep. 2018.

[13] H. Khakrah, A. Shamloo, and S. Kazemzadeh Hannani, "Exergy analysis of parabolic trough solar collectors using Al2O3/synthetic oil nanofluid," *Sol. Energy*, vol. 173, pp. 1236–1247, Oct. 2018.

[14] D. Korres, E. Bellos, and C. Tzivanidis, "Investigation of a nanofluid-based compound parabolic trough solar collector under laminar flow conditions," *Appl. Therm. Eng.*, vol. 149, pp. 366–376, Feb. 2019.

[15] M. S. Dehaj and M. Z. Mohiabadi, "Experimental investigation of heat pipe solar collector using MgO nanofluids," *Sol. Energy Mater. Sol. Cells*, vol. 191, pp. 91–99, Mar. 2019.

[16] M. A. Sharafeldin and G. Gróf, "Efficiency of evacuated tube solar collector using WO3/Water nanofluid," *Renew.*

Energy, vol. 134, pp. 453–460, Apr. 2019.

[17] M. M. Tafarroj, R. Daneshazarian, and A. Kasaeian, "CFD modeling and predicting the performance of direct absorption of nanofluids in trough collector," *Appl. Therm. Eng.*, vol. 148, pp. 256–269, Feb. 2019.

[18] Y. Xiong *et al.*, "Performance enhancement of bromide salt by nano-particle dispersion for high-temperature heat pipes in concentrated solar power plants," *Appl. Energy*, vol. 237, pp. 171–179, Mar. 2019.

[19] X. Wei, Y. Yin, B. Qin, J. Ding, and J. Lu, "Thermal conductivity improvement of liquid Nitrate and Carbonate salts doped with MgO particles," *Energy Procedia*, vol. 142, pp. 407–412, Dec. 2017.

[20] D. Shin and D. Banerjee, "Enhanced Specific Heat of Silica Nanofluid," *J. Heat Transfer*, vol. 133, no. 2, p. 024501, Feb. 2011.

[21] M. Malekan and A. Khosravi, "Investigation of Convective Heat Transfer of Ferrofluid using CFD Simulation and Adaptive Neuro-Fuzzy Inference System Optimized with Particle Swarm Optimization Algorithm," *Powder Technol.*, vol. 333, pp. 364–376, 2018.

[22] M. Malekan, A. Khosravi, and X. Zhao, "The influence of magnetic field on heat transfer of magnetic nanofluid in a double pipe heat exchanger proposed in a small-scale CAES system," *Appl. Therm. Eng.*, vol. 146, pp. 146–159, Jan. 2019.

[23] A.Jafari, T.Tynjälä, S.M.Mousavi, and P.Sarkomaa, "Simulation of heat transfer in a ferrofluid using computational fluid dynamics technique," *Int. J. Heat Fluid Flow*, vol. 29, no. 4, pp. 1197–1202, 2008.

[24] A. Khosravi and M. Malekan, "Effect of Magnetic Field on Heat Transfer Coefficient of Fe3O4-Water Ferrofluid Using Artificial Intelligence and CFD simulation," *Eur. Phys. J. Plus (under Rev.*, 2018.

[25] H. Aminfar, M. Mohammadpourfard, and F. Mohseni, "Two-phase mixture model simulation of the hydro-thermal behavior of an electrical conductive ferrofluid in the presence of magnetic fields," *J. Magn. Magn. Mater.*, vol. 324, no. 5, pp. 830–542, 2012.

[26] H. Aminfar, M. Mohammadpourfard, and Y. N. Kahnamouei, "Numerical study of magnetic field effects on the mixed convection of a magnetic nanofluid in a curved tube," *Int. J. Mech. Sci.*, vol. 78, pp. 81–90, 2014.

[27] E. Bellos, I. Daniil, and C. Tzivanidis, "Multiple cylindrical inserts for parabolic trough solar collector," *Appl. Therm. Eng.*, vol. 143, no. July, pp. 80–89, 2018.

[28] J. Muñoz and A. Abánades, "Analysis of internal helically finned tubes for parabolic trough design by CFD tools," *Appl. Energy*, vol. 88, no. 11, pp. 4139–4149, Nov. 2011.

[29] Ali Shakiba; Khodadad Vahedi, "Numerical analysis of magnetic field effects on hydro-thermal behavior of a magnetic nanofluid in a double pipe heat exchanger," *J. Magn. Magn. Mater.*, vol. 402, pp. 131–142, 2016.

[30] E. Tzirtzilakis and N. Kafoussias, "Three-dimensional magnetic fluid boundary layer flow over a linearly stretching sheet," *J. Heat Transf.*, vol. 132, no. 1, p. 011702, 2010.

[31] S. V. Mousavi, M. Sheikholeslami, M. Gorji bandpy, and M. Barzegar Gerdroodbary, "The Influence of magnetic field on heat transfer of magnetic nanofluid in a sinusoidal double pipe heat exchanger," *Chem. Eng. Res. Des.*, vol. 113, pp. 112–124, 2016.

[32] B. E. Launder and D. B. Spalding, "The numerical computation of turbulent flows," *Comput. Methods Appl. Mech. Eng.*, vol. 3, no. 2, pp. 269–289, Mar. 1974.

[33] S. E. Ghasemi and A. A. Ranjbar, "Thermal performance analysis of solar parabolic trough collector using nanofluid as working fluid: A CFD modelling study," *J. Mol. Liq.*, vol. 222, pp. 159–166, 2016.

[34] J. L. IV and J. L. V, *A Heat Transfer Textbook*, Fourth. Philogiston Press, 2012.

[35] I. Leinhard and J. Leinhard, *A Heat Tranfer Textbook*, Fourth. Saint Petersburg: Philogiston Press, 2012.

[36] P. BS, "Heat transfer in turbulent pipe flow with variable physical properties," *Harnett JP, Ed. Adv. heat Transf.*, vol. 6, pp. 504–564, 1970.

[37] A. Kasaeian, S. Daviran, R. D. Azarian, and A. Rashidi, "Performance evaluation and nanofluid using capability study of a solar parabolic trough collector," *Energy Convers. Manag.*, vol. 89, pp. 368–375, 2015.

[38] M. Sheikholeslami, F. Bani Sheykholeslami, S. Khoshhal, H. Mola-Abasia, D. D. Ganji, and H. B. Rokni, "Effect of magnetic field on Cu-water nanofluid heat transfer using GMDH-type neural network," *Neural Comput. Appl.*, vol. 25, no. 1, pp. 171–178, 2014.

[39] R. Hamilton and O. Crosser, "Thermal conductivity of heterogeneous two-component systems," *Ind. Eng. Chem.*

Fundam., vol. 1, no. 3, pp. 187–191, 1962.

[40] E. Abu-Nada, "Effects of Variable Viscosity and Thermal Conductivity of CuO-Water Nanofluid on Heat Transfer Enhancement in Natural Convection: Mathematical Model and Simulation," *J. Heat Transfer*, vol. 132, no. 5, p. 052401, 2010.

[41] K. Ravi Kumar and K. S. Reddy, "Thermal analysis of solar parabolic trough with porous disc receiver," *Appl. Energy*, vol. 86, no. 9, pp. 1804–1812, Sep. 2009.

[42] W. Siddique, I. V. Shevchuk, L. El-Gabry, N. B. Hushmandi, and T. H. Fransson, "On flow structure, heat transfer and pressure drop in varying aspect ratio two-pass rectangular channel with ribs at 45°," *Heat Mass Transf.*, vol. 49, no. 5, pp. 679–694, May 2013.

[43] W. Siddique, L. El-Gabry, I. V. Shevchuk, N. B. Hushmandi, and T. H. Fransson, "Flow structure, heat transfer and pressure drop in varying aspect ratio two-pass rectangular smooth channels," *Heat Mass Transf.*, vol. 48, no. 5, pp. 735–748, May 2012.

[44] I. V. Shevchuk, S. C. Jenkins, B. Weigand, J. von Wolfersdorf, S. O. Neumann, and M. Schnieder, "Validation and Analysis of Numerical Results for a Varying Aspect Ratio Two-Pass Internal Cooling Channel," *J. Heat Transfer*, vol. 133, no. 5, p. 051701, 2011.

[45] E. Bellos, Z. Said, and C. Tzivanidis, "The use of nanofluids in solar concentrating technologies: A comprehensive review," *J. Clean. Prod.*, vol. 196, pp. 84–99, Sep. 2018.

[46] W. RL, "Performance evaluation criteria for use of enhanced heat transfer surfaces in heat exchanger design," *Int J Heat Mass Transf*, vol. 24, pp. 715–726, 1981.

[47] E. Bellos, C. Tzivanidis, and I. Daniil, "Thermal and exergetic evaluation of parabolic trough collectors with finned absorbers operating with air," *Proc. Inst. Mech. Eng. Part A J. Power Energy*, vol. 231, no. 7, pp. 631–644, 2017.

[48] H. Olia, M. Torabi, M. Bahiraei, M. H. Ahmadi, M. Goodarzi, and M. R. Safaei, "Application of Nanofluids in Thermal Performance Enhancement of Parabolic Trough Solar Collector: State-of-the-Art," *Appl. Sci.*, vol. 9, no. 3, p. 463, Jan. 2019.

[49] L. Salgado Conrado, A. Rodriguez-Pulido, and G. Calderón, "Thermal performance of parabolic trough solar collectors," *Renew. Sustain. Energy Rev.*, vol. 67, pp. 1345–1359, 2017.

Highlights

- CFD simulation for heat transfer modeling of a parabolic trough solar collector with internal fins is carried out
- Fe_3O_4/Therminol 66 and CuO/Therminol 66 under magnetic field are proposed as working fluids
- Increasing the volume fraction and decreasing the particle size enhance the collector efficiency
- The collector efficiency with Fe_3O_4/Therminol 66 is better than CuO/Therminol 66
- The collector efficiency rises in the presence of the magnetic field